Journal of Scientific & Industrial Research
Vol. 70, July 2011, pp. 493-499

A numerical method for predicting depth of heat affected zone in EDM process for AISI H13 tool steel

M R Shabgard[1]*, M Seyedzavvar[1], S Nadimi Bavil Oliaei[2] and A Ivanov[3]
[1]Department of Mechanical Engineering, University of Tabriz, Tabriz, Iran
[2]Department of Mechanical Engineering, Middle East Technical University, Ankara, Turkey
[3]School of Engineering and Design, Brunel University, London, UK

Received 20 January 2011; revised 17 May 2011; accepted 23 May 2011

This study presents a finite element model (FEM) to model temperature distribution for AISI H13 tool steel workpiece in electrical discharge machining (EDM) at different machining parameters (pulse current, pulse on-time, temperature-sensitive material properties, size of heat source, and material flushing efficiency). Scanning electron microscopy (SEM) with energy dispersive x-ray (EDX) and micro-hardness tests were used to validate accuracy of FEM predictions. Increasing pulse on-time leads to a higher depth of heat affected zone and increasing pulse current results in a slight decrease of depth of heat affected zone. There is a good agreement between experimental and numerical results.

Keywords: Electrical discharge machining (EDM), Finite Element Model (FEM), Heat affected zone

Introduction

Electrical discharge machining (EDM), a machining process suitable to process hard materials that are difficult to machine with milling or turning, is commonly employed in aerospace, automotive, nuclear, medical and die-making industries[1,2]. [1]AISI H13 tool steel[β] justifies machining with EDM due to its high hardness. During each discharge, a crater is formed on workpiece. Depending on plasma flushing efficiency (*%PFE*), collapse of plasma channel causes very violent suction and sever bulk boiling of some of the molten material and removal from molten puddle[4]. Metal remaining in crater re-solidifies and is called recast layer. An annealed heat affected zone (HAZ) lay directly below recast layer. Both HAZ and recast layer could also contain micro-cracks. HAZ left behind by EDM process is softer than underlying material. This annealed zone could weaken prematurely and cause material to develop stress fractures that could lead to anything from a minor malfunction to a catastrophic failure. Therefore, it is imperative to revise specifications on EDM use and develop strategies to manufacture components with minimum depth of HAZ (*HD*), which involves both recast layer and underlying HAZ[5]. A number of attempts to model EDM process are reported by utilizing analytical or numerical methods[6-8]. Patel *et al*[6] applied a Gaussian-heat flux for modeling heat distribution at EDM and found model capable of providing precise quality profiles of tool wear ratio. Salah *et al*[7] presented a numerical model to study temperature distribution at EDM process and reported that temperature dependence of conductivity is of crucial importance to accuracy of numerical results and gives better correlation with experimental observations. Marafona *et al*[8] employed Finite Element Model (FEM) to estimate surface roughness and removed material from both anode and cathode.

This study presents influence of EDM input parameters [pulse current (*I*) and pulse on-time (*Ti*)] on the state of thermal distribution in HAZ of AISI H13 tool steel using software ABAQUS/CAE.

Experimental Section

Heat-distribution Modeling

Generally, differential equation for heat transfer without internal heat generation term is used as the base of thermal modeling for describing state of heat distribution during each discharge[9]. It is assumed that heat transferred to workpiece as a result of a single spark is axisymmetric and thus, equation in cylindrical coordinates is given as

*Author for correspondence
E-mail: mrshabgard@tabrizu.ac.ir

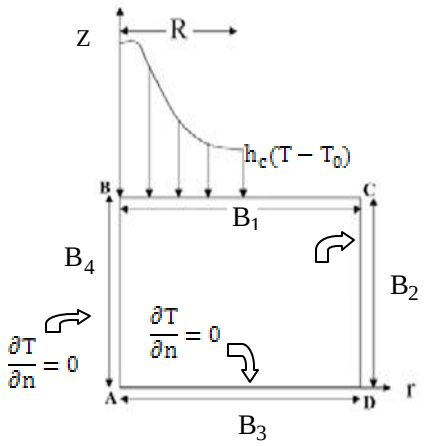

Fig. 1—Thermal model of EDM process

$$(1/r)(\partial/\partial r)(r.(\partial T/\partial r))+\partial^2 T/\partial z^2=(\rho.C/k)(\partial T/\partial t) \quad \ldots(1)$$

where T is temperature, t time, ρ, k and C are respectively density, thermal conductivity and specific heat capacity of workpiece material and r and z are coordinate axes.

Boundary and Initial Conditions

Considered domain, where heat flux is applied on surface B_1 (Fig. 1), is a small cylindrical portion of workpiece around spark. On remaining region of B_1, convention heat transfer takes place due to cooling effect by dielectric fluid. Boundaries B_2 and B_3 are very far from spark region as well spark strikes B_1 for a very little moment. Boundary B_4 is axis of symmetry, so heat flux isen taken as zero as there is no net heat gain or loss from this region[9] when t>0 as

$$BC_S: k(\partial T/\partial z) = \begin{cases} h_c(T-T_0) & r>R \\ q_w(r) & r \leq R \quad on \quad B_1 \\ 0 & for\ off\text{-}time \end{cases} \quad \ldots(2)$$

$$(\partial T/\partial n)=0 \ on \ B_2, B_3, B_4 \quad \ldots(3)$$

where, $q_w(r)$ is quantity of heat flux entering into workpiece, R is radius of spark (plasma channel), h_c is heat transfer coefficient, T_0 is room temperature and direction n is normal to the boundary.

Initial temperature T_s can be taken as T_0 of dielectric fluid, in which workpiece is submerged such as $T_s = T_0$ at $T = 0$. In addition, following assumptions have been considered: i) Model is developed for a single spark; ii) Workpiece is considered a semi-infinite body since volume of removed material is smaller than volume of workpiece; iii) Thermal effects of successive sparks on each other are neglected; iv) Effects of spark gap on discharge characteristics are negligible; v) Phase changes during analysis are neglected; vi) Crater formed on workpiece due to each discharge is assumed to have circular parabolic geometry; vii) Redeposit of recast layer in crater after each spark is considered uniform; and viii) Recast layer located outside crater redeposited on workpiece after each spark is neglected.

Analytical solution of Eq. (1) provides coordinates of points having predefined temperatures, such as melting temperature of workpiece, after specified time duration, such as pulse on-time. These points either correspond to key points that characterize crater profile (crater radius and depth), or are points on an isothermal line that may be used to define estimated crater profile. Using numerical approach, a study of evolution of isothermal lines over time may be conducted and thus, distribution of different thermally-affected zones can be obtained at any given time.

Heat Source Radius

Ikai & Hashiguchi[10] showed that radius of discharge channel is related to current intensity and pulse duration. In particular, this radius is called equivalent heat input radius and it can be expressed as a function of pulse current (I, A) and pulse on-time (Ti, μs) as $R(t) = 2.04 \times I^{0.43} \times Ti^{0.44}$, where $R(t)$ is radius of plasma channel (μm).

Heat Flux Due to Single Discharge

Gaussian heat distribution has been employed to provide more accurate results than uniform disc heat source[9]. Eq. (4) represents heat flux $q_w(r)$ at radius r[11] as

$$q_w(r)=[4.5\times F\times U_b\times I/\{p\times R^2(t)\}]\times exp[-4.5\{r/R(t)\}^2] \quad \ldots(4)$$

where U_b is breakdown (discharge) voltage, and F is a constant and represents estimated fraction of heat flux distributed to workpiece. In present study and according to Patel *et al*[6], F is considered equal to 18.3% for workpiece.

Table 1—Mechanical and physical properties of AISI H13[13]

Temperature °C	Density kg/dm^3	Specific heat J/(kg.K)	Electrical resistivity Ohm.mm^2/m	Modulus of elasticity N/mm^2	Thermal conductivity W/m.K
20	7.80	460	0.52	215×10^3	24.30
500	7.64	550	0.86	176×10^3	27.70
600	7.60	590	0.96	165×10^3	27.50
Liquidus temperature 1454			Solidus temperature 1315		

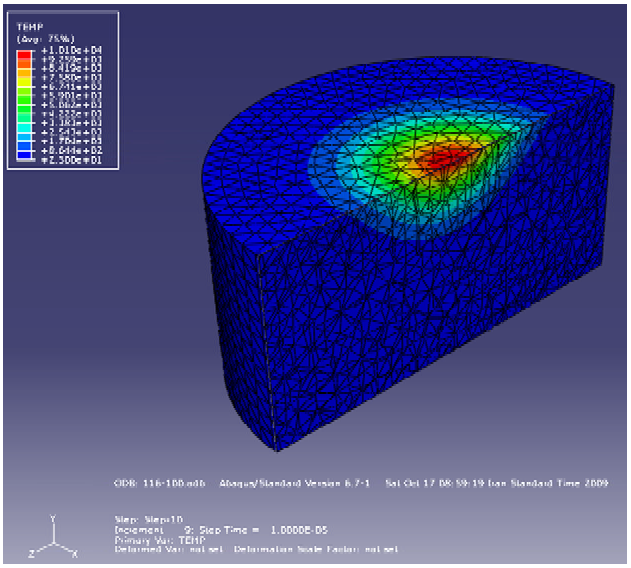

Fig. 2—3 D meshed model used in FEM

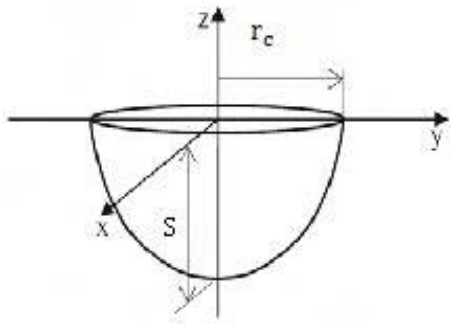

Fig. 3—Crater geometry performed by each discharge

FEM Simulation

Based on ABAQUS code, a heat transient FEM (Fig. 2) is developed to calculate temperature field in workpiece. Three dimensional (3D) finite element analyses were performed to numerically study heat distribution with respect to different machining parameter settings. Selected element type in FEM analyses is a 10-node quadratic heat transfer tetrahedron. A subroutine has been written for applying heat flux developing with time on work domain. Temperature profile obtained from FEM is used to calculate amount of material removed from specimen, exposed to heat flux. Crater formed due to each discharge can be assumed to have circular parabolic geometry[12] (Fig. 3). Theoretical crater volume defined by paraboloid geometry is described as $V_c(FEM) = ½\ \pi\ S\ r^2_c$, where $V_c(FEM)$ is volume, S is depth and r_C is radius of crater. 3D points comprised in $V_C(FEM)$ represent points over liquid temperature. Values of r_C and S were obtained by computing temperature distribution profiles along radius and depth directions of workpiece.

Experimental Procedure and Validation Methodology

Prior to ED machining, workpiece (AISI H13 tool steel) was cut in a cylindrical shape (length, 20 mm; diam, 20 mm). Main mechanical and physical properties of workpiece at different temperatures were taken as reported[13] (Table 1). Tool material was forged commercial pure copper. Machining tests were carried out at 5 *I* and 4 *Ti* settings. As a result, 20 experiments could be designed. Each machining test was performed for 15 min. Experimental test conditions were as follows: generator type, Iso pulse (ROBOFORM 200); dielectric fluid, oil flux ELF2; flashing type, normal submerged; polarity, positive; supply voltage, 200 V; reference voltage, 70 V; *I*, (8,12,16,20 & 24 A); *Ti*, (12.8, 25, 50, 100 µs); pulse interval, 6.4 µs; and tool shape, cylindrical (Ø18.3; L=20 mm).

For on-line registering the number of different kind of pulses (normal, arc, open, and short-circuit pulses) during EDM process, an oscilloscope (Hitachi VC-6524) of storage type and an electronic circuit were employed to capture gap voltage and current variations against time,

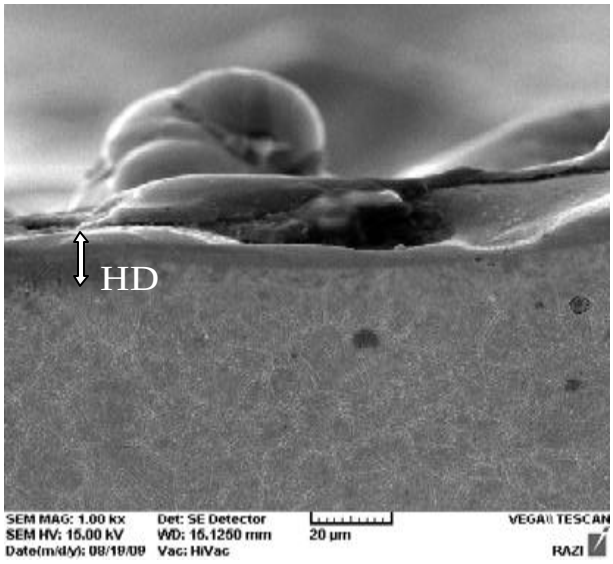

a)

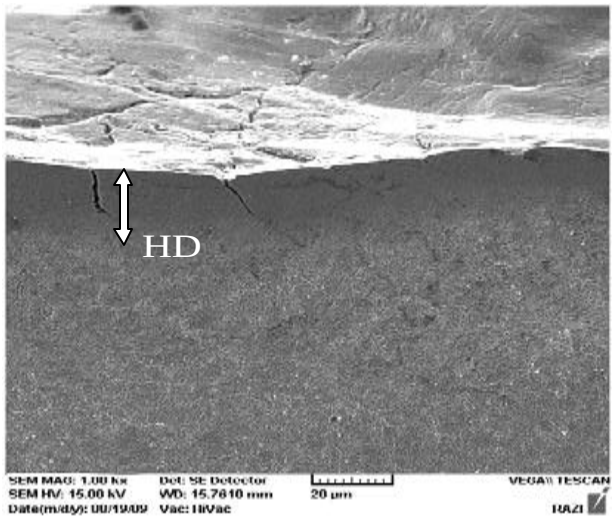

b)

Fig. 4—SEM micrograph showing cross-section of EDMed piece: a) I=8A & Ti=25µs; b) I=24A & Ti=100µs

which were then transferred and stored on a PC hard disk through a serial cable and port connection. Additionally, to count the number of each type of pulses, a program in FORTRAN language was written and linked to pulse monitoring software (ITM). A digital balance (CP2245-Surtorius) with a resolution of 0.1 mg was used for weighing workpieces and tools before and after machining process. Based on numerical results, *HD* was calculated as

$$HD = DRB - (S \times \%PFE) \quad \ldots(5)$$

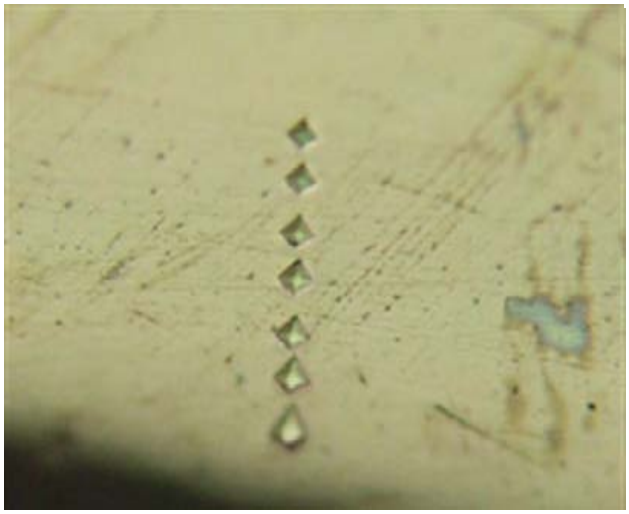

Fig. 5—Optical micrograph representing effect of penetrating point of micro-hardness tester (I=24A & Ti=100µs)

$$\%PFE = 100 \times V_C(EXP) / V_C(FEM) \quad \ldots(6)$$

$$V_C(EXP) = (M_1 - M_2) / N_{np} \times \rho \quad \ldots(7)$$

where *DRB* is depth of re-crystallization temperature border at the end of pulse on-time, *%PFE* is plasma flushing efficiency, $V_C(EXP)$ is volume of material removed per discharge obtained through empirical observation, $V_C(FEM)$ is melted volume per pulse (crater volume) predicted by FEM, M_1 and M_2 are workpiece weight before and after machining (g), respectively, N_{np} is number of normal pulses, and ñ is density of workpiece.

Empirical value of *HD* has been measured by measuring this layer's thickness at 10 different points by utilizing SEM (Fig. 4) and micro-hardness tests (Fig. 5), and accounting their average (Table 2). So machined specimens were sectioned transversely by a wirecut electrical discharge machine and prepared under a standard procedure. Etching was performed by immersing specimens in 5% Nital reagent. VEGA\\TESCAN scanning electron microscopy (SEM) and OLUMPUS LM700 micro-hardness tester were employed at this stage.

Results and Discussion

Variation of temperature with distance [along radius (Fig. 6) and depth of discharge position (Fig. 7)] are plotted for different values of *I* at *Ti* = 100µs. Key points required for calculating *HD* are represented as r_{C1}, r_{C2}, and r_{C3} (Fig. 6b), and S_1, S_2, and S_3 (Fig. 7b) as depth of

Table 2—Average depth of heat affected zone (HD) at some machining settings.

Settings	Average HD, µm	Settings	Average HD, µm
8A, 12.8µs	12.0	16A, 50µs	23.5
8A, 25µs	15.7	16A, 100µs	32.7
8A, 50µs	24	20A, 12.8µs	12
8A, 100µs	34.4	20A, 25µs	16.2
12A, 12.8µs	12.5	20A, 50µs	21.5
12A, 25µs	16.5	20A, 100µs	30.2
12A, 50µs	23	24A, 12.8µs	11
12A, 100µs	34.8	24A, 25µs	15
16A, 12.8µs	13	24A, 50µs	21
16A, 25µs	17.8	24A, 100µs	29.6

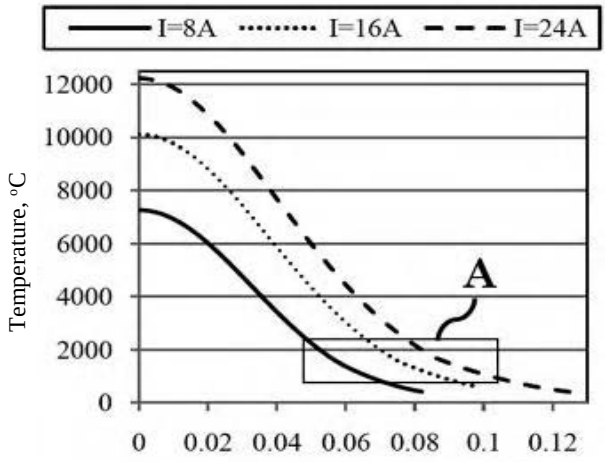

a)

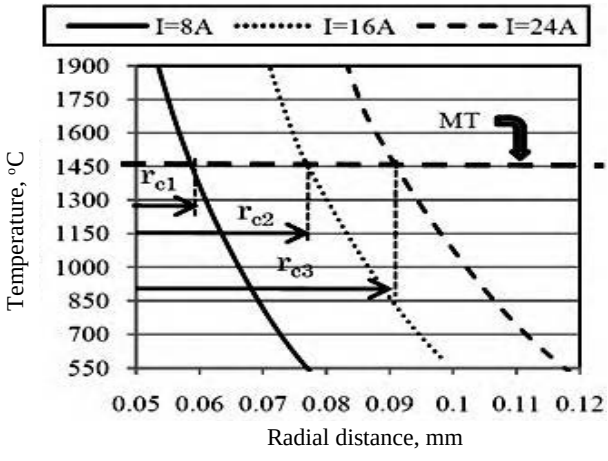

b)

Fig. 6—Temperature distribution along radial direction at: a) centerline of discharge position (Ti=100µs); b) A zone in Fig. 6a (Ti=100µs, MT=melting temp.)

molten crater and DRB_1, DRB_2, and DRB_3 (Fig. 7b) as depth of re-crystallization temperature border at the end

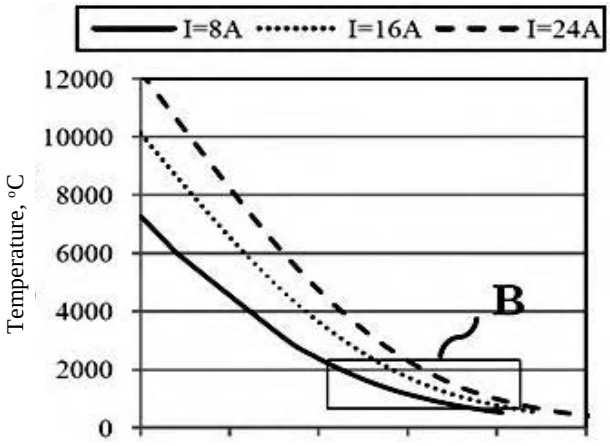

Depth from top surface at centre, mm

a)

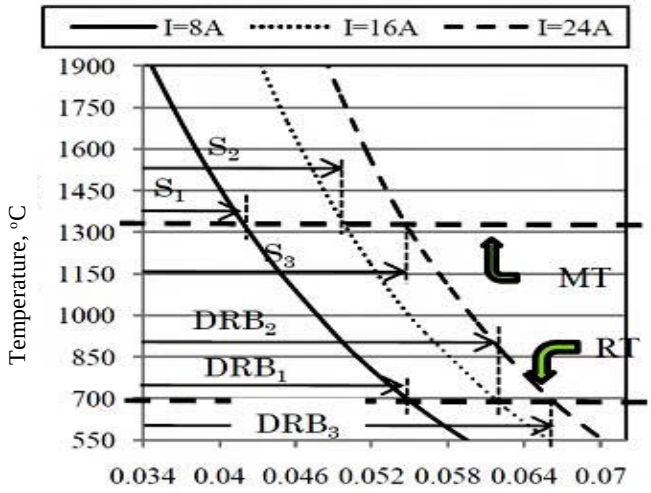

Depth from top surface at centre, mm

b)

Fig. 7—Temperature distribution along depth of workpiece at: a) centerline of discharge position (Ti=100µs); b) A zone in Fig. 7a (Ti=100µs, MT=melting temp., RT=re-crystallization temp.)

of each discharge, at different *Is*. Using these key points and Eqs (5) – (7), amount of *HD* is calculated.

FEM predicts increase of *HD* with increase of *Ti* (Fig. 8). This is justified that with increase in *Ti*, there is decrease in *PFE*. As a result, ability of plasma channel for flushing molten material from molten material crater decreases. Subsequently, this remained molten material in molten material crater re-solidifies and forms white layer upon machined surface. Furthermore, increased discharge duration results in more heat distributed into workpiece per pulse, and consequently, more underlying material is affected by high temperature. Overly, this phenomenon causes a deeper zone of heat affected area

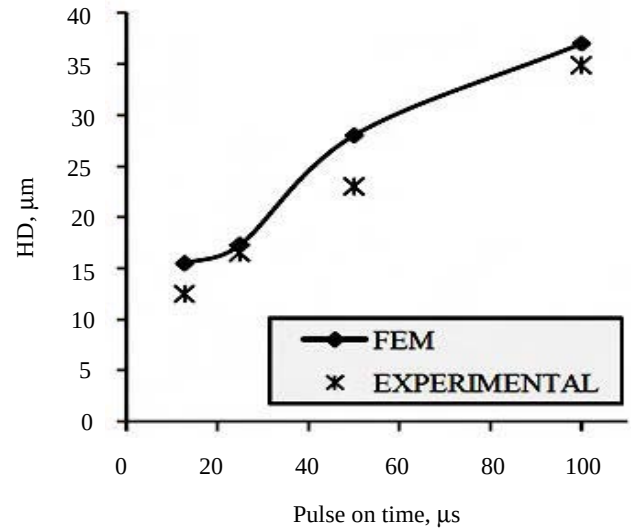

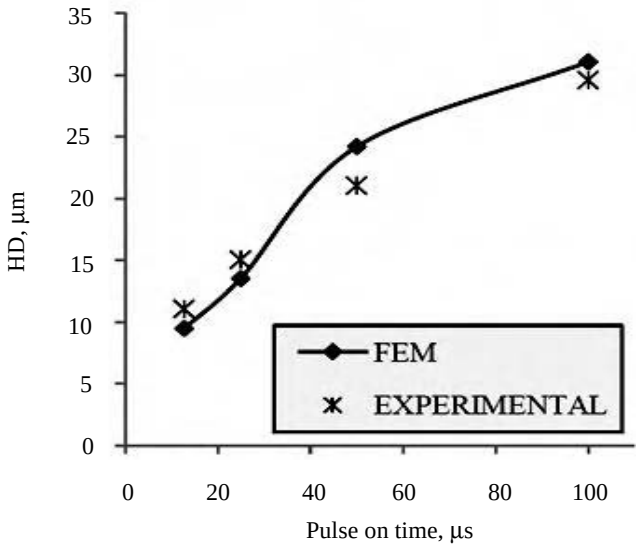

Fig 8—Heat affected zone (*HD*) depth vs pulse on time (*Ti*) at different pulse current (*I*): a) *I*= 12A; b) *I*= 24A

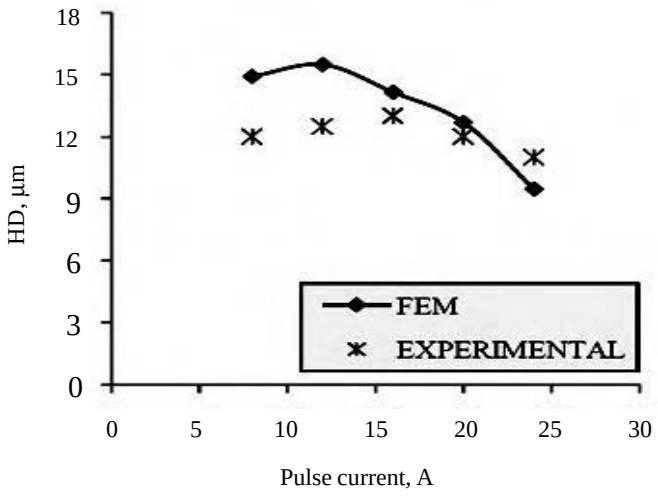

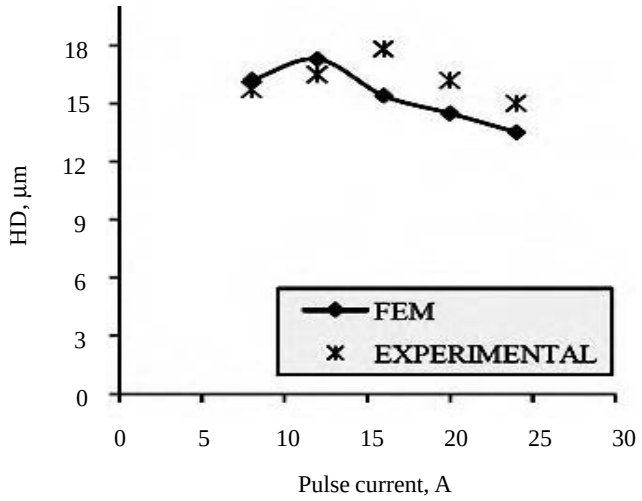

Fig 9—Heat affected zone (*HD*) depth vs pulse current (*I*) at different pulse on time (*Ti*): a) *Ti* = 12.8 µs; b) *Ti* = 25 µs

to be achieved. HD is not affected strongly by *I*, but decreases slightly by increase in its value (Fig. 9). Although increase in *I* leads to an increase in dimensions of molten crater and heat penetrating depth, *PFE* increases as *I* increases (Fig. 10). This phenomenon is explained that *%PFE* is dependent on discharge energy (W), energy changing rate (dW/dt), value of pressure of plasma channel (P), and changing rate of plasma channel pressure (dP/dt). With an increase in *I* and by constant amount of *Ti*, amount of dW/dt increases, which leads to increase in P and dP/dt. So, regarding mechanism of bulk boiling phenomenon, amount of molten material, which is ejected from molten puddle at the end of each discharge (MRR), increases and as a

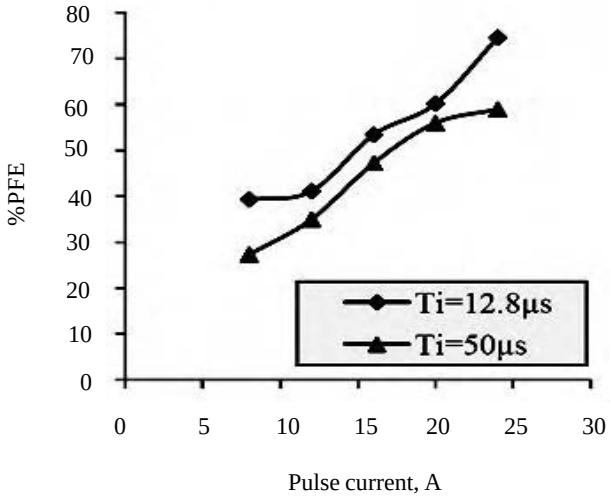

Fig. 10—Plasma flushing efficiency (*%PFE*) vs pulse current (*I*)

result, *%PFE* increases[8]. Increase in *PFE* causes more molten material to be swept away from molten crater; therefore, thinner layer of redeposit material appears on surface of workpiece. Since increase in penetrating depth of heat into workpiece and increase of *PFE* counterbalance each other's effect, *HD* does not much differ by increase in *I*.

Conclusions

Developed model can provide good prediction of *HD* in sinking-EDM process. For most of the predicted data, experimental observations agree quite well with model results. Leading conclusions of presented FEM and experimental results are as follows: i) Increase in pulse on-time leads to an increase in *HZ*; ii) Slight decrease could be observed in *HZ* by an increase in pulse current; and iii) HAZ produced by short pulse duration and long pulse duration have not similar depth values when pulse energies are almost same; rather low pulse on-time leads to reduction in *HZ*.

Acknowledgement

Authors are indebted to Razi Metallurgical Laboratory, Metallurgical Laboratory of Sahand University of Technology, universal workshop of Educational Center of Iran Tractor Manufacturing Company, and advance machining workshop of Manufacturing Engineering Department of University of Tabriz. Also, authors appreciate the help of Prof J Khalil Allafy, Prof T B Navid Chakharlu and Mr A Nejat Ebrahimi for technical support.

References

1 Ho K H & Newman S T, State of the art electrical discharge machining (EDM), *Int J Mach Tool Manuf*, **43** (2003) 1287-1300.

2 Abdullah A & Shabgard M R, Effect of ultrasonic vibration of tool on electrical discharge machining of cemented tungsten carbide (WC-Co), *Int J Adv Manuf Technol*, **38** (2008) 1137-1147.

3 Castro G, Fernandez-Vicente A & Cid J, Influence of the nitriding time on the wear behaviour of an AISI H13 steel during a crankshaft forging process, *J Wear*, **263** (2007) 1375-1385.

4 Dibitonto D D, Eubank P T, Patel M R & Barrufet M A, Theoretical models of the electrical discharge machining process. I. A simple cathode erosion model, *J Appl Phys*, **66** (1989) 4095-4103.

5 Rebelo J C, Marao D A, Kremer D & Lebrun J L, Influence of EDM pulse energy on the surface integrity of martensitic steels, *J Mater Process Technol*, **84** (1998) 90-96.

6 Patel M R, Barrufet M A, Eubank P T & Dibitonto D D, Theoretical models of the electrical discharge machining process. II. The anode erosion model, *J Appl Phys*, **66** (1989) 4104-4111.

7 Ben S N, Ghanem F & Ben A K, Numerical study of thermal aspects of electric discharge machining process, *Int J Mach Tool Manuf*, **46** (2006) 908-911.

8 Marafona J & Chousal J A G, A finite element model of EDM based on Joule effect, *Int J Mach Tool Manuf*, **46** (2006) 595-602.

9 Yadav V, Jain V K & Dixit P M, Thermal stress due to electrical discharge machining, *Int J Mach Tool Manuf*, **42** (2007) 877-888.

10 Ikai T & Hashigushi K, *Heat input for crater formation in EDM*, in *Proc Int Symp for Electro-Machining- ISEM XI* (EPFL, Lausanne, Switzerland) 1995, 163-170.

11 Hargrove S K & Ding D, Determining cutting parameters in wire EDM based on workpiece surface temperature distribution, *Int J Adv Manuf Technol*, **34** (2007) 296-299.

12 Salonitis K, Stournaras A, Stavropoulos P & Chryssolouris G., Thermal modeling of the material removal rate and surface roughness for die-sinking EDM, *Int J Adv Manuf Technol*, **40** (2009) 316-323.

13 http://www.bohler-edelstahl.at